

# Polarizability and Screening in Chiral Multilayer Graphene

Hongki Min<sup>1</sup>, E. H. Hwang<sup>2</sup>, and S. Das Sarma<sup>2</sup>

<sup>1</sup>*Department of Physics and Astronomy, Seoul National University, Seoul 151-747, Korea*

<sup>2</sup>*Condensed Matter Theory Center, Department of Physics,  
University of Maryland, College Park, Maryland 20742, USA*

(Dated: February 13, 2012)

We calculate the static polarizability of multilayer graphene and study the effect of stacking arrangement, carrier density, and onsite energy difference on graphene screening properties. At low densities, the energy spectrum of multilayer graphene is described by a set of chiral two-dimensional electron systems and the associated chiral nature determines the screening properties of multilayer graphene showing very different behavior depending on whether the chirality index is even or odd. As density increases, the energy spectrum follows that of the monolayer graphene and thus the polarizability approaches that of monolayer graphene. The qualitative dependence of graphene polarizability on chirality and layering indicates the possibility of distinct graphene quantum phases as a function of the chirality index.

Since the discovery of graphene in 2004, experimental fabrication of gated graphene, it has been a subject of great interest[1]. Recently, multilayer graphene has attracted considerable attention for its fundamental properties and chiral electronic structure, and for future applications due to the presence of additional layer degree of freedom. Interestingly, the electronic structure of multilayer graphene is sensitive to its stacking sequences[2, 3], indicating the possibility of engineering electronic properties by tuning the stacking arrangement. Optical properties of multilayer graphene have been studied experimentally[4] and theoretically[5], showing that characteristic peak positions in the optical conductivity depend on stacking sequences. Transport properties of multilayer graphene depend sensitively on the number of layers and stacking sequences in the system[6]. Quantum Hall effects in trilayer graphene show different quantization rules compared with monolayer and bilayer graphene[7]. Electron-electron interactions also play an important role in multilayer graphene, especially in periodic ABC stacking compared with other stacking sequences due to the appearance of relatively flat bands near the Fermi energy indicating the possibility of interaction induced ordered states[8] which could be very different from those studied in monolayer and bilayer graphene.

As the number of graphene layers increases, effects of screening become more and more important due to the enhancement of the electronic density of states (DOS), which determines the fundamental properties such as transport, optical properties, phonon dispersion, and RKKY interaction. The energy band structure of multilayer graphene is very sensitive to its stacking sequence, leading to its screening properties depending strongly on the stacking arrangements. There has been extensive theoretical activity on Coulomb screening in monolayer[9] and bilayer graphene[10], but there is no systematic study whatsoever of screening in multilayer graphene.

In this Letter, we calculate the static polarizability of multilayer graphene and systematically study the effect of stacking arrangement, carrier density, and onsite

energy difference on its screening properties. We first study the screening properties of a chiral two-dimensional electron system (C2DES) with an arbitrary chirality  $J$  demonstrating that the polarizability and the associated screening behavior strongly depend on  $J$  due to the enhanced (suppressed) backscattering for even (odd)  $J$ . Next we calculate the screening properties of multilayer graphene, and then compare and analyze the results using those of C2DES. At low densities, the energy spectrum of multilayer graphene is described by a set of C2DESs[3] and screening is determined by its chiral nature. As density increases, the energy spectrum eventually follows that of monolayer graphene and thus the polarizability approaches that of monolayer graphene in the high density limit. We also show that the onsite energy difference between the sublattices or layers, which could induce a band gap, can enhance or suppress the backscattering depending on the chiral nature of multilayer graphene.

The static polarizability is defined by

$$\Pi(\mathbf{q}) = -g \sum_{\lambda, \lambda'} \int \frac{d^2k}{(2\pi)^2} \frac{f_{\lambda, \mathbf{k}} - f_{\lambda', \mathbf{k}'}}{\varepsilon_{\lambda, \mathbf{k}} - \varepsilon_{\lambda', \mathbf{k}'} + i0^+} F_{\lambda, \lambda'}(\mathbf{k}, \mathbf{k}'), \quad (1)$$

where  $g = g_s g_v$  is the total degeneracy factor ( $g_s = g_v = 2$  are spin and valley degeneracy factors, respectively),  $\varepsilon_{\lambda, \mathbf{k}}$  and  $f_{\lambda, \mathbf{k}}$  are the eigenenergy and Fermi function for the band index  $\lambda$  and wavevector  $\mathbf{k}$ , respectively,  $F_{\lambda, \lambda'}(\mathbf{k}, \mathbf{k}')$  is the square of the wavefunction overlap between  $|\lambda, \mathbf{k}\rangle$  and  $|\lambda', \mathbf{k}'\rangle$  states, and  $\mathbf{k}' = \mathbf{k} + \mathbf{q}$ .

To understand the screening properties of multilayer graphene, we first consider a 2-band pseudospin Hamiltonian which describes 2D chiral quasiparticles[3]. The pseudospin Hamiltonian with the chirality index  $J$  is of the form

$$H_J(\mathbf{k}) = t_{\perp} \begin{pmatrix} 0 & \left(\frac{\hbar v_0 k_-}{t_{\perp}}\right)^J \\ \left(\frac{\hbar v_0 k_+}{t_{\perp}}\right)^J & 0 \end{pmatrix}, \quad (2)$$

where  $k_{\pm} = k_x \pm i k_y$ ,  $v_0$  is the effective in-plane

Fermi velocity and  $t_\perp$  is the nearest-neighbor inter-layer hopping. The Hamiltonian has an energy spectrum given by  $\varepsilon_{s,\mathbf{k}} = st_\perp \left( \frac{\hbar v_0 |\mathbf{k}|}{t_\perp} \right)^J$  and corresponding eigenfunctions are  $|s, \mathbf{k}\rangle = \frac{1}{\sqrt{2}} (s, e^{iJ\phi_{\mathbf{k}}})$ , where  $\phi_{\mathbf{k}} = \tan^{-1}(k_y/k_x)$  and  $s = \pm 1$  for positive (negative) energy states, respectively. Note that for C2DEs,  $F_{s,s'}(\mathbf{k}, \mathbf{k}') = \frac{1}{2} [1 + ss' \cos J(\phi_{\mathbf{k}} - \phi_{\mathbf{k}'})]$ , thus the backscattering with  $\phi_{\mathbf{k}} - \phi_{\mathbf{k}'} = \pm\pi$  between the same bands  $s = s'$  is enhanced (suppressed) for even (odd)  $J$  due to the chiral nature of the electronic structure. This has important consequences as scattering properties of odd/even  $J$  turn out to be qualitatively different.

To investigate the polarizability we rewrite Eq. (1) as  $\Pi(q) = \Pi_{\text{intra}}(q) + \Pi_{\text{inter}}(q)$ , where the intraband polarizability  $\Pi_{\text{intra}}$  is defined by the intraband transition terms  $\lambda = \lambda'$  in Eq. (1), and the interband polarizability  $\Pi_{\text{inter}}$  with  $\lambda \neq \lambda'$  in Eq. (1) which is induced by the virtual interband transitions.

For the undoped intrinsic case (with the carrier density  $n$  being zero), we find  $\Pi_{\text{intra}}(q) = 0$  and  $\Pi_{\text{inter}}(q) = N(q)I(J)$ , where  $N(q) = \frac{q q^{2-J}}{2\pi J t_\perp (\hbar v_0/t_\perp)^J}$  and  $I(J)$  is a constant depending only on the chirality index  $J$ , given by

$$I(J) = J \int_0^\infty x dx \int_0^{2\pi} \frac{d\phi}{2\pi} \frac{1 - \cos(J\theta)}{x^J + (x')^J}, \quad (3)$$

where  $x' = \sqrt{1 + 2x \cos \phi + x^2}$ , and  $\cos \theta = (x + \cos \phi)/x'$ . For example, we have  $I(1) = \pi/8$  and  $I(2) = \log 4$ . Note that the screened Coulomb potential is given by  $V_{\text{sc}}(q) = 2\pi e^2 / [\kappa (q + q_s(q))]$ , where  $\kappa$  is the background dielectric constant and  $q_s(q) = (2\pi e^2 / \kappa) \Pi(q)$  is the screening wavevector. For the intrinsic case,  $q_s(q) \propto q^{2-J}$ , and thus in the long wavelength limit, the screened Coulomb potential behaves as  $V_{\text{sc}}(q) \propto q^{J-2}$  and for  $J \geq 3$  it vanishes as  $q \rightarrow 0$ , whereas  $V_{\text{sc}}(q) \propto 1/q$  as  $q \rightarrow \infty$  for all  $J$ . Thus, the long wavelength Coulomb interaction is completely screened for  $J \geq 3$ .

Next we consider the polarizability for the doped extrinsic case (i.e.  $n \neq 0$ ). At  $q = 0$ , the polarizability becomes the DOS at Fermi energy  $\varepsilon_F$ , i.e.  $\Pi(0) = N(\varepsilon_F) \equiv N_0$  where  $N(\varepsilon) = \frac{q t_\perp}{2\pi J (\hbar v_0)^2} (|\varepsilon|/t_\perp)^{\frac{J}{2}-1}$  is the DOS at energy  $\varepsilon$  for C2DES. Note that in the intrinsic limit ( $n \rightarrow 0$ , or equivalently  $\varepsilon_F \rightarrow 0$ ),  $N_0$  diverges as  $\varepsilon_F^{\frac{J}{2}-1}$  or  $n^{1-\frac{J}{2}}$  for  $J \geq 3$ , which indicates enhanced screening at low densities. In Fig. 1(a) the Thomas-Fermi (TF) screening wavevector,  $q_{\text{TF}} = q_s(q = 0) = (2\pi e^2 / \kappa) \Pi(q = 0)$ , is shown as a function of density, in which  $q_{\text{TF}} \propto N_0 \propto n^{1-\frac{J}{2}}$  diverges as  $n \rightarrow 0$  for  $J \geq 3$ . For comparison, we also show the TF screening wavevector for multilayer graphene in Fig. 1(b). At low densities, the energy spectrum of multilayer graphene is described by a set of C2DEs[3], and the C2DES with the largest chirality dominates the DOS and the screening wavevector. Note that the periodic ABC-stacked  $J$ -layer graphene, whose energy spectrum is described by  $J$  C2DES at low

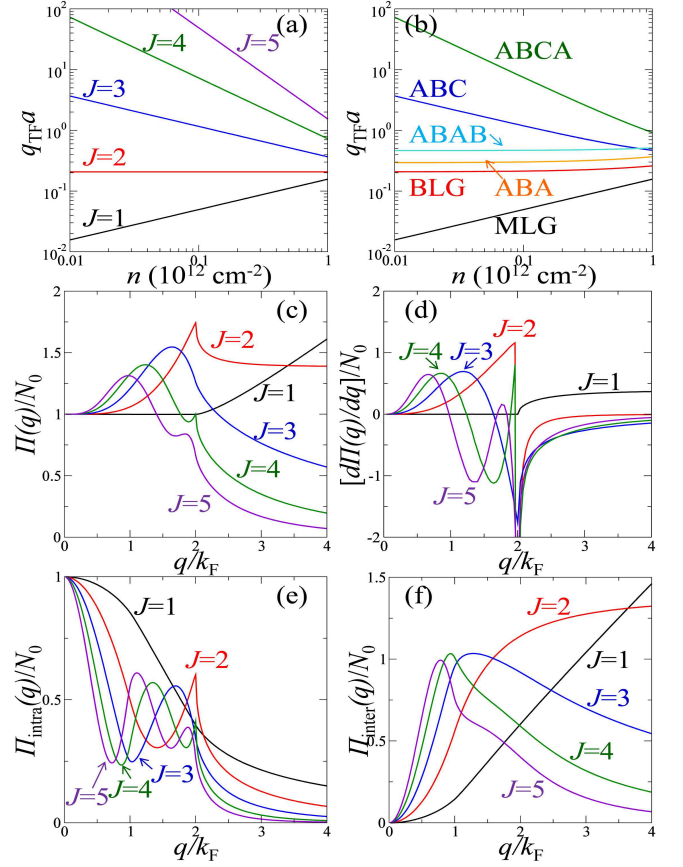


FIG. 1. (a) The Thomas-Fermi wavevector,  $q_{\text{TF}} \propto N_0 = \Pi(q = 0)$ , as a function of density  $n$  with  $\kappa = 2.5$ , where  $a = 0.246$  nm is the lattice constant of graphene. (b) Same as (a) for multilayer graphene with several stacking sequences, where MLG and BLG represent monolayer and bilayer graphene, respectively. (c) and (d) show the total static polarizability  $\Pi(q)$  and its first derivative  $d\Pi(q)/dq$ , respectively, as a function of wavevector for C2DES with chiralities  $J = 1, 2, 3, 4, 5$ . Note that the first derivative at  $2k_F$  is continuous (discontinuous) for odd (even)  $J$ . (e) and (f) show the intraband and interband polarizabilities, respectively.

densities, shows divergent screening behavior for  $J \geq 3$ .

Figure 1(c) shows the total static polarizability as a function of wavevector for C2DES. We note that the normalized polarizabilities of Fig. 1(c) vary in orders of magnitude depending on  $J$  if they are expressed in absolute units, as indicated in Fig. 1(a). In Fig. 1(d) the first derivative of the total polarizability with respect to the wavevector,  $d\Pi(q)/dq$ , is shown for each  $J$ . In Figs. 1(e) and (f) we show the intraband and interband polarizabilities for several chirality indices  $J = 1, 2, 3, 4, 5$ , respectively.

For small  $q$ , the polarizability becomes

$$\begin{aligned} \Pi_{\text{intra}}(q) &= N_0 \left[ 1 - \frac{J^2 q^2}{8k_F^2} + O(q^4) \right], \\ \Pi_{\text{inter}}(q) &= N_0 \frac{J^2 q^2}{8k_F^2} \left[ 1 - \frac{J[(J-1)^2 - 5]}{16(J+2)} \frac{q^2}{k_F^2} + O(q^4) \right]. \end{aligned} \quad (4)$$

As  $q$  increases,  $\Pi_{\text{intra}}$  ( $\Pi_{\text{inter}}$ ) decreases (increases) quadratically in the leading order and these quadratic leading order terms exactly cancel out in the total polarizability. Thus, the total polarizability increases slowly as  $q^4$  except for  $J = 1$ , where two terms exactly cancel out up to  $q = 2k_F$  giving a constant 2D polarizability for  $q \leq 2k_F$ . For large  $q$ , we have  $\Pi_{\text{intra}} = N_0 [(J/2)(q/k_F)^{-J} + O(q^{-J-1})]$  and  $\Pi_{\text{inter}} = N_0 [I(J)(q/k_F)^{2-J} + O(q^{-J})]$ . Thus for large wavevectors  $q \gg 2k_F$ , the polarizability from interband transition dominates, and  $\Pi(q) \approx \Pi_{\text{inter}}(q)$ .

Since many significant physical properties (e.g. transport, Kohn anomaly, and quantum criticality) are induced by the behavior of the polarizability at  $q = 2k_F$ , we look further into  $\Pi(q)$  near  $q = 2k_F$ . At  $q = 2k_F$ , the calculated polarizability with even  $J$  shows a cusp while that with odd  $J$  varies continuously with  $q$  appearing as an inflection point in  $\Pi(q)$ . As  $q$  approaches  $2k_F$  from above we find  $\Pi(q) \propto (q^2 - 4k_F^2)^{3/2}$  for odd number of  $J$  and  $\Pi(q) \propto (q^2 - 4k_F^2)^{1/2}$  for even number of  $J$ . As a consequence, the static polarizability has a discontinuous (continuous) first derivative for even (odd)  $J$  [see Fig. 1(d)]. For even  $J$ s the first derivative is discontinuous at  $q = 2k_F$  showing  $d\Pi(q)/dq \propto 1/\sqrt{q^2 - 4k_F^2}$ , while for odd  $J$ s, the discontinuity appears in the second derivative as  $d^2\Pi(q)/dq^2 \propto 1/\sqrt{q^2 - 4k_F^2}$ . The origin of these singular features is closely related to  $2k_F$  backscattering in the system. When the contribution of the  $2k_F$  scattering to the polarizability is enhanced due to the chiral property of even  $J$  (or the overlap factor in Eq. (1)), the polarizability has a singular feature, whereas when the backscattering is suppressed for odd  $J$ , no singular features occur. Note that all these singular properties arise only from the intraband polarizability.

So far we have studied the polarizability for a simple two band model of 2D chiral quasiparticles. Now we consider the polarizability for a full band continuum model of multilayer graphene near the hexagonal corners of the Brillouin zone, called the  $K$  and  $K'$  points, taking into account only nearest-neighbor intralayer hopping  $t$  and the nearest-neighbor interlayer hopping  $t_\perp$ . In this paper  $t = 3$  eV and  $t_\perp = 0.3$  eV will be used in numerical calculations.

Figure 2(a) shows the polarizability of zero-gap bilayer graphene as a function of wavevector for several carrier densities with the energy band structure as an inset. For small densities, the polarizability of the full four band model resembles that of the  $J = 2$  C2DES (top black line). As the density increases, the polarizability eventually approaches that of monolayer graphene because at high densities the interlayer coupling becomes negligible and the energy band structure behaves like a collection of monolayer graphene sheets. The main difference between the polarizability of monolayer and high density bilayer graphene is the existence of a kink at  $q = 2k_F$ , which arises from the enhanced backscattering and does not vanish completely in bilayer graphene even at very high densities, i.e. the system maintains its memory even

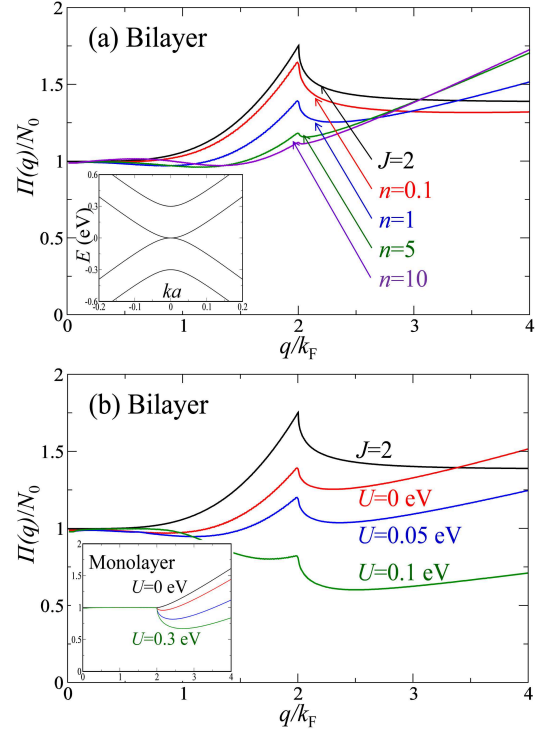


FIG. 2. (a) Static polarizability of bilayer graphene with the zero energy gap as a function of wavevector for several carrier densities in units of  $10^{12} \text{ cm}^{-2}$ . The inset of (a) shows the energy band structure of bilayer graphene. In (b) we include the onsite energy difference  $U$  between the layers to open the energy gap. The polarizability is calculated for a carrier density  $n = 10^{12} \text{ cm}^{-2}$  and for different values of  $U$ . In both figures the black solid line corresponds to the result of C2DES with  $J = 2$ . The inset of (b) shows the static polarizability of monolayer graphene with energy differences between the two sublattices of  $U = 0, 0.1, 0.2, 0.3$  eV.

at very high carrier density where the energy dispersion has become the same as that in monolayer graphene.

Figure 2(b) shows the static polarizability of bilayer graphene with an onsite energy difference between the layers for a fixed density  $n = 10^{12} \text{ cm}^{-2}$ . As the onsite energy difference increases, the energy band gap also increases, reducing the interband contribution and the overall magnitude of the polarizability. Note that in the presence of the onsite energy difference, the backscattering is suppressed and thus the cusp structure at  $2k_F$  becomes weakened. In case of monolayer graphene, however, the onsite energy difference between the two *sublattices* gives rise to the enhanced backscattering in addition to the opening of an energy gap. As a consequence, the polarizability of monolayer graphene with the onsite energy difference develops a cusp structure at  $2k_F$ , as shown in the inset of Fig. 2(b). This can be understood if we consider the effect of the onsite energy difference on the overlap factor in Eq. (1), which weakens the enhancement (suppression) of the backscattering for doped bilayer (monolayer) graphene. Therefore, depending on

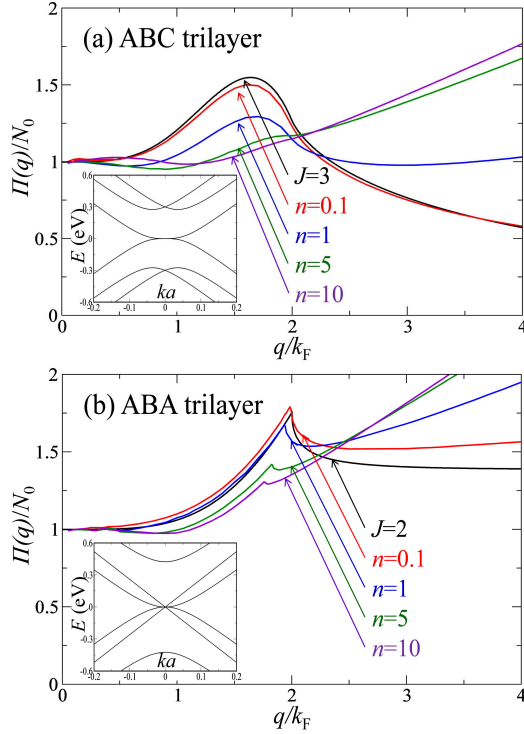


FIG. 3. Calculated polarizability as a function of wavevector with several densities in units of  $10^{12} \text{ cm}^{-2}$  for (a) ABC trilayer graphene and (b) ABA trilayer graphene. The black line in (a) and (b) indicates the result of C2DES with  $J = 3$  and  $J = 2$ , respectively. Insets show the energy band structure of each stacking.

the chiral properties of multilayer graphene, the onsite energy difference may enhance or weaken the backscattering and the cusp structure at  $2k_F$ .

In Fig. 3 the polarizability of trilayer graphene is shown with the energy band structure as an inset. Excluding consecutive stacking sequences, there are two distinct stacking arrangements, ABC and ABA in trilayer graphene. Figure 3(a) shows the polarizability of ABC trilayer graphene as a function of wavevector. Note that for ABC stacking the low-energy spectrum is described by  $J = 3$  C2DES. For comparison, we also show the polarizability of  $J = 3$  C2DES (top black line). At low densities, the polarizability resembles that of the low-energy C2DES with  $J = 3$  for ABC trilayer, while as the density increases, it approaches that of monolayer graphene. Figure 3(b) is the same as Fig. 3(a) but for ABA trilayer graphene. Note that at low densities ABA trilayer graphene is described by a direct product of  $J = 1$  and  $J = 2$  C2DEs and the Fermi energy crosses two energy bands at  $k_{F1}$  and  $k_{F2}$  corresponding to the  $J = 1$  and  $J = 2$  energy bands, respectively. Thus the ABA trilayer graphene has two different Fermi wavevectors which can be calculated from the carrier density  $n = \frac{q}{4\pi} k_F^2 = \frac{q}{4\pi} (k_{F1}^2 + k_{F2}^2)$ . The polarizability of ABA trilayer graphene in Fig. 3(b) appears to be qualitatively different from that of ABC trilayer graphene. One sig-

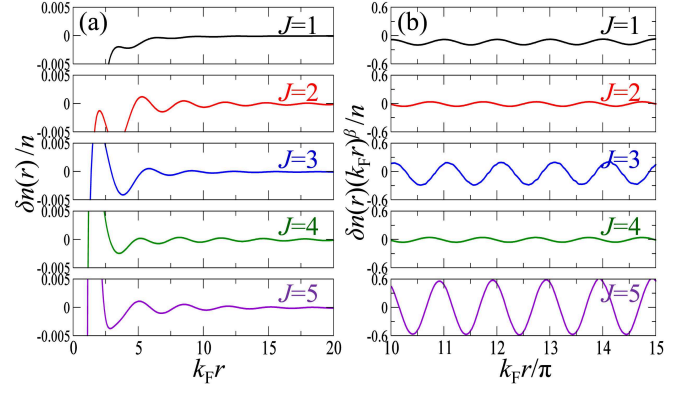


FIG. 4. (a) Density oscillations of C2DES with chiralities  $J = 1, 2, 3, 4, 5$  using RPA for  $n = 10^{12} \text{ cm}^{-2}$  with  $\kappa = 2.5$ . In (b)  $\delta n(r)$  is rescaled by  $r^\beta$  where  $\beta = 2$  ( $\beta = 3$ ) for even (odd)  $J$ , which clearly shows the decaying pattern at large distances with the periodicity of  $\pi/k_F$ .

nificant feature is the existence of a cusp at  $2k_{F2}$  instead of  $2k_F$ . As the density increases, the cusp becomes weakened and it shifts because the ratio  $k_{F2}/k_F$  decreases. This peculiar feature can be understood from the DOS of ABA trilayer graphene. Since the DOS of  $J = 2$  C2DES is larger than that of  $J = 1$  C2DES at small energies (i.e.,  $N(\epsilon) \propto \epsilon^{\frac{2}{3}-1}$ ) many physical properties of ABA stacking trilayer graphene are determined by  $J = 2$  C2DES. Thus for low densities the polarizability resembles that of the  $J = 2$  C2DES and the cusp structure appears at  $2k_{F2}$ .

Similar analysis can be applied to arbitrarily stacked multilayer graphene and we can easily generalize the results of bilayer and trilayer graphene discussed so far. At low densities, the energy spectrum of multilayer graphene is described by a set of C2DEs and the polarizability behaves as that of a C2DES with the largest chirality. As the density increases, the polarizability follows that of monolayer graphene because the energy spectrum behaves like a collection of monolayer graphene sheets. In the presence of the onsite energy difference, the backscattering may be enhanced or suppressed depending on the chiral nature of the system, giving enhanced or suppressed cusp structure at  $2k_F$ .

One direct consequence of the polarizability function we have calculated is the density fluctuation induced by a point charge which is given by

$$\delta n(r) = \int \frac{q dq}{2\pi} J_0(qr) [\epsilon^{-1}(q) - 1], \quad (5)$$

where  $J_0(x)$  is the zeroth-order Bessel function and  $\epsilon(\mathbf{q})$  is the static dielectric function, which is given by  $\epsilon(\mathbf{q}) = 1 + \frac{2\pi e^2}{\kappa q} \Pi(\mathbf{q})$  within the random phase approximation (RPA). Figure 4(a) shows the calculated density oscillations of C2DES for  $n = 10^{12} \text{ cm}^{-2}$  with  $\kappa = 2.5$ . At large distance ( $k_F r \gg 1$ ) we find a density oscillation (Friedel oscillation) which has the form  $\sin(2k_F r)/r^2$  for even  $J$  while  $\cos(2k_F r)/r^3$  for odd  $J$ , as seen in Fig. 4(b). This

radial decaying pattern arises from the kink structure at  $2k_F$  of the polarizability function. When the discontinuity appears in the first (second) derivative of the polarizability,  $d\Pi(q)/dq$  ( $d^2\Pi(q)/dq^2$ ), the radial decay has a form of  $r^{-2}$  ( $r^{-3}$ ). The discontinuity of the derivative is the direct consequence of the enhanced (suppressed) backscattering for even (odd)  $J$ . One interesting aspect

of the polarizability of C2DES, which is reflected in these Friedel oscillations as well as in the screening properties, is that even (odd)  $J$  behaves like qualitatively similarly to the Lindhard polarization function for 2D (3D) electron gas systems.

This work is supported by the NRI-SWAN and US-ONR.

- 
- [1] S. Das Sarma, S. Adam, E. H. Hwang, and E. Rossi, *Rev. Mod. Phys.* **83**, 407 (2011).
  - [2] S. Latil and L. Henrard, *Phys. Rev. Lett.* **97**, 036803 (2006); F. Guinea, A. H. Castro Neto, and N. M. R. Peres, *Phys. Rev. B* **73**, 245426 (2006); B. Partoens and F. M. Peeters, *Phys. Rev. B* **75**, 193402 (2007); M. Koshino and T. Ando, *Phys. Rev. B* **76**, 085425 (2007).
  - [3] Hongki Min and A. H. MacDonald, *Phys. Rev. B* **77**, 155416 (2008); Hongki Min and A. H. MacDonald, *Prog. Theor. Phys. Suppl.* **176**, 227 (2008).
  - [4] K. F. Mak, M. Y. Sfeir, J. A. Misewich, T. F. Heinz, arXiv:0908.0154 (unpublished); K. F. Mak, J. Shan, and T. F. Heinz, *Phys. Rev. Lett.* **104**, 176404 (2010).
  - [5] C. L. Lu, C. P. Chang, Y. C. Huang, R. B. Chen, and M. L. Lin, *Phys. Rev. B* **73**, 144427 (2006); M. Koshino and T. Ando, *Solid State Commun.* **149**, 1123 (2009); Hongki Min and A. H. MacDonald, *Phys. Rev. Lett.* **103**, 067402 (2009).
  - [6] J. Nilsson, A. H. Neto, F. Guinea, and N. M. Peres, *Phys. Rev. Lett.* **97**, 266801 (2006); Hongki Min, P. Jain, S. Adam, and M. D. Stiles, *Phys. Rev. B* **83**, 195117 (2011); Hongki Min, E. H. Hwang, and S. Das Sarma, *Phys. Rev. B* **83**, 161404(R) (2011).
  - [7] T. Taychatanapat, K. Watanabe, T. Taniguchi, and P. Jarillo-Herrero, *Nature Physics* **7**, 621 (2011); W. Bao, L. Jing, J. Velasco Jr, Y. Lee, G. Liu, D. Tran, B. Standley, M. Aykol, S. B. Cronin, D. Smirnov, M. Koshino, E. McCann, M. Bockrath, and C. N. Lau, *Nature Physics* **7**, 948 (2011); L. Zhang, Y. Zhang, J. Camacho, M. Khodas, and I. Zaliznyak, *Nature Physics* **7**, 953 (2011).
  - [8] F. Zhang, B. Sahu, Hongki Min, and A. H. MacDonald, *Phys. Rev. B* **82**, 035409 (2010).
  - [9] E. H. Hwang and S. Das Sarma, *Phys. Rev. B* **75**, 205418 (2007); T. Ando, *J. Phys. Soc. Jpn.* **75**, 074716 (2006); B. Wunsch, T. Stauber, F. Sols, and F. Guinea, *New J. Phys.* **8**, 318 (2006); Y. Barlas, T. Pereg-Barnea, M. Polini, R. Asgari, and A. H. MacDonald, *Phys. Rev. Lett.* **98**, 236601 (2007); L. Brey, H. A. Fertig, and S. Das Sarma, *Phys. Rev. Lett.* **99**, 116802 (2007).
  - [10] E. H. Hwang and S. Das Sarma, *Phys. Rev. Lett.* **101**, 156802 (2008); X.-F. Wang and T. Chakraborty, *Phys. Rev. B* **75**, 041404(R) (2007); G. Borghi, M. Polini, R. Asgari, and A. H. MacDonald, *Phys. Rev. B* **80**, 241402(R) (2009); R. Sensarma, E. H. Hwang, and S. Das Sarma, *Phys. Rev. B* **82**, 195428 (2010).